Check for updates

Solar RRL
www.solar-rrl.com

Optical Optimization Potential of Transparent-Passivated Contacts in Silicon Solar Cells

Alexander Eberst, Alexandr Zamchiy, Kaifu Qiu, Peter Winkel, Habtamu T. Gebrewold, Andreas Lambertz, Weiyuan Duan, Shenghao Li, Karsten Bittkau, Thomas Kirchartz, Uwe Rau, and Kaining Ding*

Herein, an optical loss analysis of the recently introduced silicon carbide–based transparent passivating contact (TPC) for silicon heterojunction solar cells is presented, the most dominant losses are identified, and the potential for reducing these losses is discussed. Magnesium fluoride is applied as an antireflective coating to reduce the reflective losses by up to 0.8 mA cm^{-2}. When applying the magnesium fluoride, the passivation quality of the layer stack degrades, but is restored after annealing on a hot plate in ambient air. Afterwards, a road map for TPC solar cells toward an efficiency of 25% is presented and discussed. The largest part in efficiency gain is achieved by reducing the finger width and by increasing the passivation quality. Furthermore, it is shown that TPC solar cells have the potential to achieve short-circuit current densities above 42 mA cm^{-2} if the finger width is reduced and the front-side indium tin oxide (ITO) layer can be replaced by an ITO silicon nitride double layer.

1. Introduction

To keep the rise in efficiency of crystalline silicon (c-Si) solar cells going, a multitude of approaches are currently under investigation to realize the combination of spatial separation of the metal contacts from the silicon wafer and effective passivation of the c-Si surface, while also maximizing the incident light and keeping good contact properties. Promising approaches are the use of either polycrystalline silicon (poly-Si)[1] or hydrogenated amorphous silicon (a-Si:H),[2] called silicon heterojunction (SHJ), for passivation and charge carrier extraction purposes. Due to the absorption coefficient of these materials being similar to that one of crystalline silicon (c-Si), one severe limitation in these approaches is the large loss of incident light in these layers, called parasitic absorption,[3,4] and thus a limited short-circuit current density J_{SC}. This parasitic absorption could be mitigated by the so-called Interdigitated Back Contact (IBC) approach, where both the electron and hole contact are placed on the non-illuminated rear side of the c-Si. By using this structure, the incident light is maximized and the parasitic absorption minimized, but the fabrication process of IBC cells is more complex.[5–7]

To keep the contacts at the illuminated side of the cell and thus the fabrication process simpler, a broad spectrum of materials is currently under investigation to fulfill the initially mentioned criteria. Metal compounds like zinc oxide or molybdenum oxide[8] or different silicon-based materials like microcrystalline silicon[9,10] are promising approaches. Another silicon-based, highly transparent material is hydrogenated nanocrystalline silicon carbide (nc-SiC:H), which was recently introduced in a contact scheme called transparent passivating contact (TPC).[11] The TPC combines a thin wet-chemically grown silicon oxide as tunnel oxide[12,13] with a nitrogen-doped nc-SiC:H double layer to achieve a high

A. Eberst, K. Qiu, P. Winkel, H. T. Gebrewold, A. Lambertz, W. Duan, S. Li, K. Bittkau, T. Kirchartz, U. Rau, K. Ding
IEK-5 Photovoltaics
Forschungszentrum Jülich GmbH
52425 Jülich, Germany
E-mail: a.eberst@fz-juelich.de

A. Eberst, P. Winkel, H. T. Gebrewold, U. Rau
Faculty of Electrical Engineering and Information Technology
RWTH Aachen University
52074 Aachen, Germany

The ORCID identification number(s) for the author(s) of this article can be found under https://doi.org/10.1002/solr.202101050.

© 2022 The Authors. Solar RRL published by Wiley-VCH GmbH. This is an open access article under the terms of the Creative Commons Attribution License, which permits use, distribution and reproduction in any medium, provided the original work is properly cited.

DOI: 10.1002/solr.202101050

A. Zamchiy
Novosibirsk State University
630090 Novosibirsk, Russia

A. Zamchiy
Kutateladze Institute of Thermophysics SB RAS
630090 Novosibirsk, Russia

K. Qiu
Institute for Solar Energy Systems
Guangdong Provincial Key Laboratory of Photovoltaic Technology
School of Physics
Sun Yat-Sen University
Guangzhou 510275, P.R. China

T. Kirchartz
Faculty of Engineering and CENIDE
University of Duisburg-Essen
47057 Duisburg, Germany

transparency in combination with excellent passivation, leading to a certified efficiency of 23.8% without an additional antireflective coating and 24.0% efficiency with said coating.[11] Additionally, the fabrication process of the TPC is very lean.[14]

This work focusses on the optical losses of the certified 23.8% efficiency TPC cell and identifies its mayor contributors. After the optical losses are identified, an in-depth analysis beyond the previous study[11] of the influence of MgF_2 as antireflective coating is presented. We discuss the problems and present a possible solution, leading to the certified efficiency of 24.0%. In the following, we give a possible pathway to achieve efficiencies of 25% using TPC and elaborate on the potential of the TPC to reach a J_{SC} of 42 mA cm^{-2}.

2. Optical Properties and Losses in the TPC Cell

2.1. Optical Loss Analysis

Figure 1 shows the optical loss analysis of the 23.8% TPC solar cell, as shown in Figure S1, Supporting Information, without MgF_2[11] according to Paviet-Salomon et al..[15] For the loss analysis, we use in-house measured external quantum efficiency (EQE), reflectance (R_{cell}), and transmission (T_{cell}) curves of the cell, as well as reflectance curves, which we simulate using the online tool OPAL2 (R_{OPAL2}). We calculate the losses from finger shading from the finger geometry, as explained in the Supporting Information. While the absorption losses in the near-infrared wavelength regime (2.4 mA cm^{-2}) and the losses from finger shading (1.5 mA cm^{-2}) are the most severe ones, the losses from front surface escape (1.1 mA cm^{-2}) and reflection (0.8 mA cm^{-2}), as well as the other wavelength dependent losses in the blue wavelength regime (0.6 mA cm^{-2}) and intermediate wavelength regime (0.1 mA cm^{-2}), also play a big role in reducing the J_{SC}. No losses from transmission through the cell occur due to the fully metalized rear side of the cell.

While most of these losses are complicated to reduce since other solar cell parameters will also be influenced when changing the corresponding properties, we show how to reduce the reflection losses with a straightforward approach, which is to introduce an additional antireflective coating layer, which reduces the refractive index difference between two adjacent layers, in this case, the ITO and air. MgF_2 is a suitable material, as already commonly used in SHJ cells to reduce the reflection,[8] since its refractive index n_{MgF2} for wavelength from 300 to 1200 nm is between 1.3 and 1.4, which is between the refractive index of ITO with $1.62 \leq n_{ITO} \leq 2.51$ and air with $n_{air} = 1$. Additionally, MgF_2 has an absorption coefficient of nearly zero for visible light, thus the parasitic absorption will not increase significantly. The measurements are all conducted in air. It is expected that, in a module, the short-circuit current gain from MgF_2 is likely less than in air, if there is any gain at all. Nevertheless, the use of MgF_2 as antireflective coating shows the potential of the TPC and if the encapsulation material in a module can match the refractive index of MgF_2, a similar effect might be achieved in a module as well.

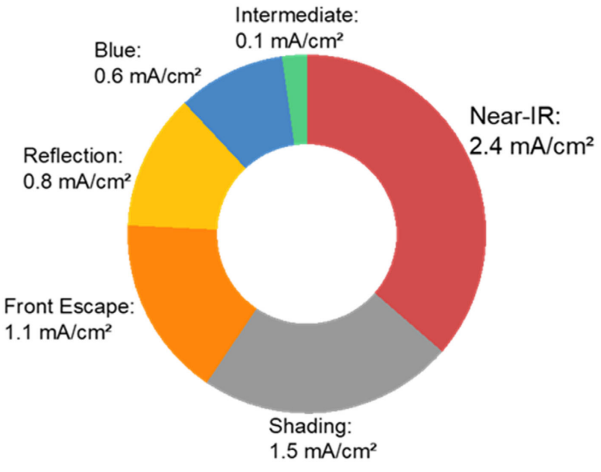


Figure 1. Optical losses in the transparent passivating contact cell according to Paviet-Salomon et al.[15] The biggest contributors to the losses are the long-wavelength near-IR absorption losses, followed by losses from finger shading and front escape.

2.2. Optical Optimization

In **Figure 2**, it is shown that adding a MgF_2 layer reduces the reflectance of a TPC test cell. The reflection is notably reduced below a wavelength of 500 nm and between 600 and 1000 nm. This reduction in reflection increases absorption and thus leads to a higher EQE.

The calculated short-circuit current gain from the reduced reflection from the difference in the measured reflection curve is ≈0.8 mA cm^{-2}, while the calculated short-circuit current gain in *EQE* only equals ≈0.15 mA cm^{-2}. The lower short-circuit current gain in *EQE* than from the reduced reflection is an indication for a reduction in the quality of the passivation, which is also shown in the current-voltage (IV) parameters of the test cell in **Table 1**. There it can be seen that the V_{OC}, the *pFF*, and also the Fill Factor (*FF*) decrease, leading also to a reduction in efficiency after the MgF_2 evaporation.

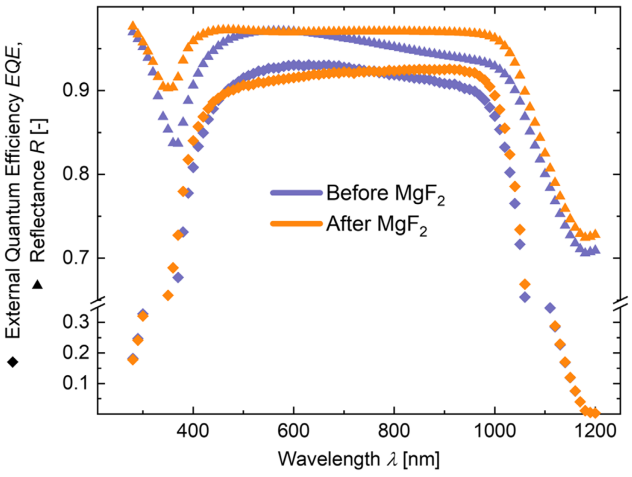


Figure 2. Reflectance measurement and external quantum efficiency (*EQE*) measurement of the transparent passivating contact (TPC) before and after MgF_2, but without any annealing. There is a mismatch from the calculated short-circuit current gain from the reduced reflection and the gain in *EQE*.

© 2022 The Authors. Solar RRL published by Wiley-VCH GmbH

2367198x, 2022, 6, Downloaded from https://onlinelibrary.wiley.com/doi/10.1002/solr.202101050 by Universitatsbibliothek RWTH Aachen University, Wiley Online Library on [19/02/2026]. See the Terms and Conditions (https://onlinelibrary.wiley.com/terms-and-conditions) on Wiley Online Library for rules of use; OA articles are governed by the applicable Creative Commons License

Table 1. In-house measured parameters for a transparent passivating contact (TPC) test solar cell and the champion cell before and after the MgF_2 evaporation and after subsequent annealing. Also, the simulated cell data of the champion cell using Quokka 3 is shown.

		Efficiency η [%]	J_{SC} [mA cm^{-2}]	V_{OC} [mV]	*FF* [%]	*pFF* [%]	R_S [Ω cm]
Test cell	Before MgF_2 evaporation	23.1	40.0	716	80.5	84.1	0.757
	After MgF_2 evaporation	22.6	40.2	710	79.3	82.9	0.791
	After annealing	23.5	40.52	718	80.7	84	0.693
Champion cell	Before MgF_2 evaporation	23.6	40.1	727	80.8	83.9	0.731
	After MgF_2 evaporation	23.8	40.9	723	80.4	83.8	0.732
	After annealing	24.0	40.9	726	80.7	83.8	0.684
Simulated champion cell (Quokka 3)		23.88	40.9	725.5	80.48	—	0.501

The lower short-circuit current gain and reduced V_{OC} are signs for a lower passivation quality and could be explained by more unpassivated dangling bonds, which act as energetic states in the band gap of the c-Si surface. They act as traps for the charge carriers in which the carriers recombine. When more charge carriers recombine, for example, through these trap states, the V_{OC} and the generated current is reduced, possibly explaining the difference in calculated gain from the reflectance and *EQE*. The drop in *FF* can be explained by the drop in *pFF*, which also stems from the reduced passivation quality and thus enhanced recombination.[16,17] A reduction caused by an increase in R_S can be ruled out since R_S is approximately constant, as can be seen for example in **Figure 3**e. A possible mechanism for the degradation of the passivation is given at the end of this chapter.

The TPC test cell was placed on a hot plate in ambient air for various times and temperatures after the MgF_2 evaporation, as indicated on the x-axis of Figure 3. As shown in Figure 3a–d,

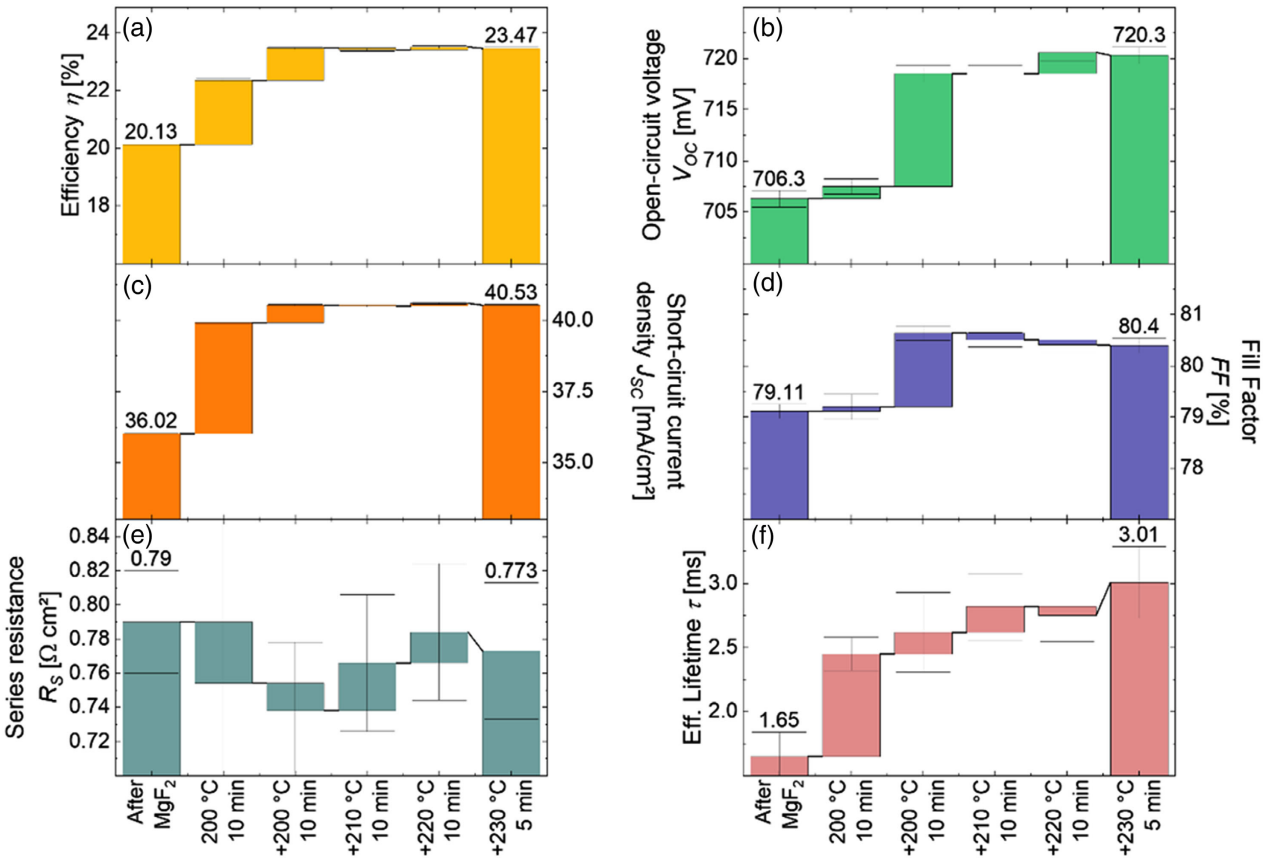


Figure 3. a) Efficiency η, b) J_{SC}, c) V_{OC}, d) *FF*, e) R_S, and f) τ_{eff} of a TPC cell for different annealing steps on a hot plate in ambient air. The annealing time and temperature can be found on the *x*-axis. After the first two annealing steps, we observe no further enhancement of the performance parameters of the solar cell.

© 2022 The Authors. Solar RRL published by Wiley-VCH GmbH

2367198x, 2022, 6, Downloaded from https://onlinelibrary.wiley.com/doi/10.1002/solr.202101050 by Universitatsbibliothek RWTH Aachen University, Wiley Online Library on [19/02/2026]. See the Terms and Conditions (https://onlinelibrary.wiley.com/terms-and-conditions) on Wiley Online Library for rules of use; OA articles are governed by the applicable Creative Commons License

after the first annealing step, there is a large increase in J_{SC} of 3.89 mA cm^{-2} and only small increases in *FF* and V_{OC}. *FF* and V_{OC} have a significant increase of 1.44%$_{abs}$ and 11 mV, respectively, after the second annealing step. Within the measurement error, the V_{OC}, J_{SC}, and *FF* are constant for any further annealing step. The error in *FF* and fluctuation for the different annealing steps might be explained by the sheet resistance R_S, which error is extraordinarily large and stems from the measurement tool. The recovered passivation can be seen in the increased V_{OC} as well as the steady increase in effective lifetime τ_{eff}, in Figure 3f where an increased lifetime implies lower recombination losses and thus a better passivation.

As shown in previous studies,[11] the first two annealing steps were then applied to the champion cell. The efficiency was improved from 23.8% to 24.0%, mainly by improving the J_{SC} to 40.9 mA cm^{-2} while maintaining the *FF* and the V_{OC}. The in-house measured history for each cell parameter for each processing step of the test cell and the champion cell can be found in Table 1.

As a possible explanation, we suggest that in the initial passivation directly after the nc-SiC:H(n) growth, atomic hydrogen introduced during the deposition process might passivate the dangling bonds of the crystalline silicon interface that are not bonded to oxygen of the SiO_X tunnel oxide layer. The degradation of the passivation during the MgF_2 evaporation could be due to cracking of silicon–hydrogen bonds at the crystalline silicon interface, leading to more dangling bonds and an increased recombination. It is very unlikely that particles reach the crystalline silicon interface during the MgF_2 evaporation, since for example during a sputtering process, oxygen ions with an energy of 1 keV would only penetrate ≈4 nm into silicon.[18] The thermal energy kT of the MgF_2 at the evaporation temperature T, calculated by using the melting point of MgF_2, $T = 1528$ K,[19] and k being the Boltzmann constant, is ≈0.66 eV. One explanation could be thermally induced cracking of the silicon–hydrogen bonds at the c-Si interface. Since no additional heater is used, the energy might come from impacting particles or radiation emitted from the sublimation process of the MgF_2 and is then transported to the SiO_X/c-Si interface by lattice vibrations, which can transport energies up to 75 meV.[20] The heat supplied during the annealing then restores some of the previously broken bonds. The underlying assumption is that a single hydrogen atom can't persist and needs a bonding partner, in this case either a silicon dangling bond, saturating another silicon bond either at the c-Si interface, or from the SiO_X, or another hydrogen, forming H_2. Once detached from the silicon dangling bond of the crystalline silicon interface and, if bonded to another hydrogen atom, the H_2 diffuses mostly along the c-Si interface, since SiO_2 decreases the hydrogen diffusion significantly.[21–23] Since the oxide grown here is most likely under-stoichiometric,[24,25] some hydrogen might escape from the interface and is lost for passivation purposes. The other H_2 molecules remain close to the dangling bonds of the c-Si interface and can be reused for passivation purposes when cracked during the annealing procedure, re-saturating said dangling bond. A schematic visualization of the resulting lifecycle on the hydrogen at the interface can be found in Figure S4, Supporting Information.

3. Potential of the TPC

3.1. Efficiency Road Map to 25%

We used the data from the certified solar cell with an efficiency of 24.0% from previous studies[11] as a base to find input parameters for a simulation using QUOKKA3 of the certified cell. The simulation allowed us to obtain further insights into losses of the solar cell and enables us to design a road map describing the path toward achieving efficiencies of 25% with TPCs. **Figure 4** presents the breakdown of the different losses resulting from our QUOKKA3 simulations. For the analysis, two main assumptions had to be made. The current losses were multiplied by the simulated voltage at the maximum power point to convert them in mW cm^{-2} for an easier comparison between current (optical) losses and free energy (recombination, resistive) losses. The reflection losses were estimated from OPAL2 simulations and the absorption in the different layers was approximated from Lambert–Beer law. The optical losses are the most dominant ones with total losses of 3.38 mW cm^{-2}, whereas the total recombination losses are 1.49 mW cm^{-2} and total resistive losses are 1.02 mW cm^{-2}. In the optical losses, 1.63 mW cm^{-2} are lost by unabsorbed photons, while 0.97 mW cm^{-2} are lost from finger shading. In the recombination losses, 0.78 mW cm^{-2} is lost from recombination at the front c-Si interface and 0.42 mW cm^{-2} at the rear c-Si interface. Unabsorbed photons are photons with energies above the band-gap E_g, but with energies low enough that they are not fully absorbed during the pass-through of the silicon bulk. These photons are either reflected or parasitically absorbed, e.g., in the near-IR regime or at the metallization, and thus do not contribute to electron-hole pair generation. The individual resistive losses are all rather small.

Subsequently, we adapted the simulation of the base cell to decrease the mayor loss contributors to achieve a final efficiency of 25%. Note that the simulated base efficiency deviates slightly from the certified efficiency. This discrepancy is because most IV parameters of the cell could be matched in addition to R_S and thus a slight mismatch in *FF* could not be avoided. But as can be seen by the large error bars in Figure 3e, the measured R_S value are not too precise. Also, a slight deviation in the simulated and measured V_{OC} could not be avoided.

The final road map can be found in **Figure 5**, where the changes in the simulation are marked. An extended explanation of the changed simulation parameters can be found in the Supporting Information. Reducing the finger width will reduce the losses from the finger shading and can be done by adjusting the screen-printing process. Simultaneously, the finger pitch needs to be adjusted to avoid losses in the *FF*. A balance between a reduced finger width for increasing the incident light and a smaller finger pitch to mitigate losses in the R_S and *FF* needs to be found to increase the J_{SC} and maintain the *FF*. The surface recombination velocity at the front c-Si surface $S_{eff,front}$ could be reduced by an additional hydrogenation step or optimization of the wet-chemical oxidation process of the SiO_X. Preliminary experiments have already shown that an increase in implied V_{OC} of up to 7 mV, suggesting a lower $S_{eff,front}$, can be achieved by adjusting the concentrations of hydrogen peroxide and sulfuric acid during the wet-chemical oxidation of the wafers, probably changing the reaction kinetics and thus growing a more

© 2022 The Authors. Solar RRL published by Wiley-VCH GmbH

2367198x, 2022, 6, Downloaded from https://onlinelibrary.wiley.com/doi/10.1002/solr.202101050 by Universitatsbibliothek RWTH Aachen University, Wiley Online Library on [19/02/2026]. See the Terms and Conditions (https://onlinelibrary.wiley.com/terms-and-conditions) on Wiley Online Library for rules of use; OA articles are governed by the applicable Creative Commons License

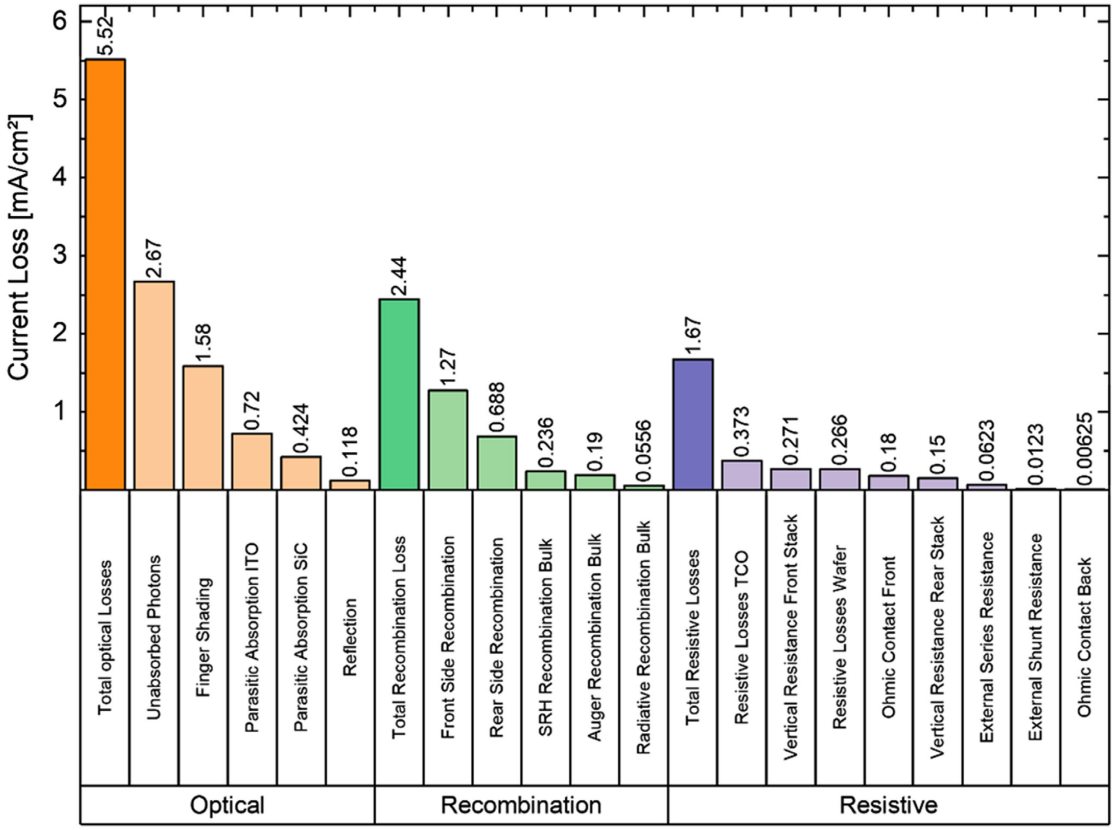


Figure 4. Loss Analysis using QUOKKA3 of the certified 24.0% cell from previous studies.[11] To see the influence of the losses on the short-circuit current density, the losses are given in mA cm^{-2}. If the tool gives the losses in mW cm^{-2}, they are divided by V_{MPP} to estimate the losses in mA cm^{-2}.

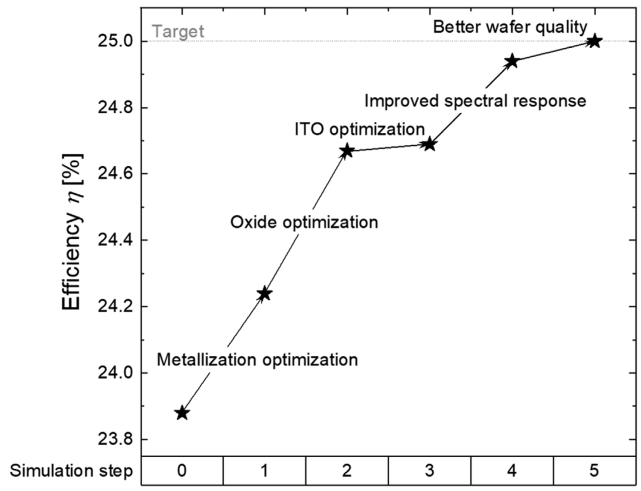


Figure 5. Simulated road map to a solar cell efficiency of 25% with a TPC on the front side. The changes compared to the base simulation, which is of the certified 24.0% cell from previous studies,[11] are noted in the graph. Adjusting the front finger structure and reducing $S_{eff,front}$ contribute most to an increased efficiency.

stoichiometric oxide. The bulk lifetime is determined by the quality of the wafers. The near-IR response can be increased by, for example, decreasing the near-IR absorption in the front stack. One possibility would be to replace the transparent conductive oxide (TCO) with higher mobility TCO materials, which have a better trade-off of optoelectrical performance, such as hydrogenated indium oxide (IO:H) or titanium-doped indium oxide (ITiO). The absorptance of IO:H is equal to or lower than that of ITO, especially for wavelength above 600 nm.[26] The absorption coefficient of ITiO can be found in Figure S2, Supporting Information. It is similar to that of ITO until wavelength of approximately 350 nm and significantly lower than that of ITO for wavelength above 350 nm. Here, it is important that the electrical properties of the new TCO are similar to that of the ITO so that the gain from the previous optimization stays valid.

3.2. J_{SC} Potential of the TPC

Based on the certified cell in previous studies,[11] the J_{SC} can be optimized for a potential $J_{SC,pot}$ of 42 mA cm^{-2}. The biggest gain of the missing 1.1 mA cm^{-2} can come from the reduced finger width and optimized finger pitch mentioned in the previous section. By halving the finger width from currently 60 to 30 µm, which is still doable by screen printing or copper plating, the simulations show a gain in $J_{SC,pot}$ of 0.6 mA cm^{-2}.

For the last 0.5 mA cm^{-2}, an optical Sentaurus technology computer aided design (TCAD) simulation was performed to further optimize the J_{SC}. **Figure 6**a shows the potential of improving

© 2022 The Authors. Solar RRL published by Wiley-VCH GmbH

2367198x, 2022, 6, Downloaded from https://onlinelibrary.wiley.com/doi/10.1002/solr.202101050 by Universitatsbibliothek RWTH Aachen University, Wiley Online Library on [19/02/2026]. See the Terms and Conditions (https://onlinelibrary.wiley.com/terms-and-conditions) on Wiley Online Library for rules of use; OA articles are governed by the applicable Creative Commons License

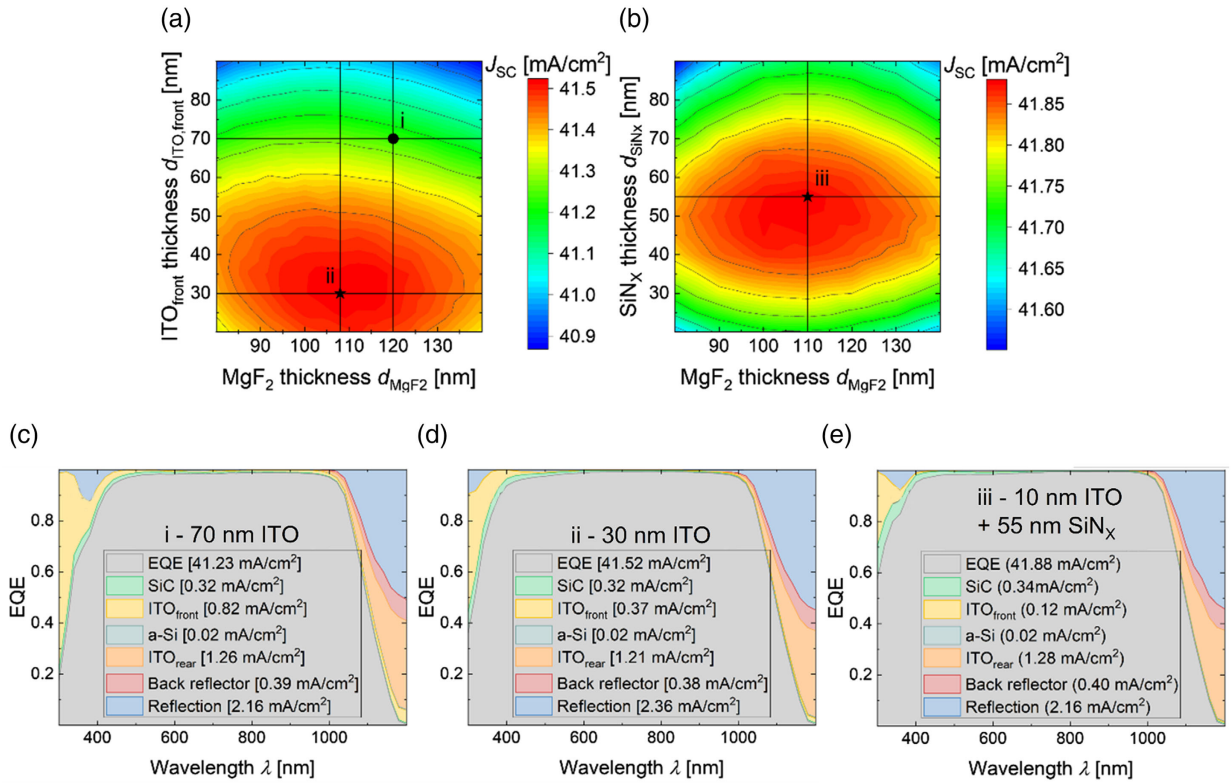


Figure 6. Sentaurus TCAD simulations for the optical optimization of a cell using the TPC on the front side. a) Heatmap of the J_{SC} depending on the thickness of the ITO and of the MgF_2. The previously used thicknesses are marked with a circle, while the thicknesses for optically optimized layers are marked with a star. b) Heatmap of the J_{SC} depending on the thickness of SiN_X and MgF_2 with 10 nm of ITO under the SiN_X. The J_{SC}-optimized layer thicknesses are marked with a star. Simulated optical losses for each layer for the c) current layer thicknesses, d) the optimized thicknesses using only ITO, and e) the optimized thicknesses using the layer stack ITO (10 nm)/SiN_X/MgF_2. By reducing the ITO thickness and adding 55 nm SiN_X as ARC, a gain in J_{SC} of 0.65 mA cm^{-2} can be achieved.

the efficiency by optimizing the ITO. With an original ITO thickness of 70 and 120 nm of MgF_2, 0.82 mA cm^{-2} is parasitically absorbed in the front ITO, while 2.16 mA cm^{-2} is lost by reflection, as shown in Figure 6c. When the ITO thickness is reduced and the MgF_2 thickness is adjusted accordingly, the parasitic absorption is reduced but the antireflective properties of the ITO are decreased as well, also leading to a higher reflection loss of 2.34 mA cm^{-2}. When optimizing the $J_{SC,pot}$ gain from reduced parasitic absorption versus the $J_{SC,pot}$ loss from the increased reflectance, a total gain of 0.29 mA cm^{-2} can be achieved, originating from reducing parasitic absorption in the ITO to 0.37 mA cm^{-2} with an increased reflection loss of 2.36 mA cm^{-2}, as shown in Figure 6d compared to Figure 6c. The total gain by only an optimized ITO layer thickness is insufficient to achieve a theoretical $J_{SC,pot}$ of 42.00 mA cm^{-2} because of the inherent trade-off between antireflective properties and parasitic absorption. Fortunately, in a broad wavelength regime, silicon nitride (SiN_x) has a comparable refractive index (as shown in Figure S3, Supporting Information) to ITO when grown under the right conditions.[27] Unlike ITO, the absorption coefficient of SiN_x is negligible. When the ITO layer is set to 10 nm to reduce the parasitic absorption and still maintain some of the electrical properties, Figure 6b shows that an additional 55 nm of SiN_X in combination with 110 nm MgF_2 is needed for optimal antireflective properties. Figure 6e shows that with the ITO/SiN_X/MgF_2 anti-reflection coating (ARC), the parasitic absorption can be reduced to 0.12 mA cm^{-2} while maintaining the low reflection losses from the current case. According to the simulations, this would enable an additional gain in J_{SC} of 0.65 mA cm^{-2}, for a total $J_{SC,pot,max}$ of 42.15 mA cm^{-2}. Unfortunately, the sheet resistance of the ITO increases with decreasing thickness. According to electrical simulations, this leads to a reduced *FF* of 79.43% and 77.63% for 30 and 10 nm ITO, respectively. The gain in J_{SC} can't completely compensate the lower *FF* and the efficiency is reduced to 23.7% and 23.3% for 30 and 10 nm ITO, respectively. This could be counteracted by further optimizing the conductivity of the conductive nc-SiC:H(n) layer.[28] Li et al. have shown that the TCO can be completely omitted and that the c-Si wafer can be used for lateral conduction if the contact resistance is sufficiently low.[29]

4. Conclusion

In this work, the optical losses of the recently introduced TPC[11] are analyzed using numerical simulations and experiments. An antireflective MgF_2 layer, which has a refractive index between that of ITO and air, can reduce the reflective losses, which constitute a significant fraction of the overall optical losses.

© 2022 The Authors. Solar RRL published by Wiley-VCH GmbH

2367198x, 2022, 6, Downloaded from https://onlinelibrary.wiley.com/doi/10.1002/solr.202101050 by Universitatsbibliothek RWTH Aachen University, Wiley Online Library on [19/02/2026]. See the Terms and Conditions (https://onlinelibrary.wiley.com/terms-and-conditions) on Wiley Online Library for rules of use; OA articles are governed by the applicable Creative Commons License

We observe experimentally that evaporating the antireflective layer onto the cell reduces its V_{OC} and *pFF*. Furthermore, the calculated gain from the reduced reflection is lower than the calculated gain from a higher *EQE*. These reductions can be explained by a reduced quality of the passivation, probably attributed to the hydrogen distribution. After annealing two times at 200 °C in ambient air for 10 min, the reduced parameters can be recovered. After curing, a high J_{SC} of 40.9 mA cm^{-2} can be achieved.

We perform a full loss analysis, including optical, recombination, and resistive losses, using the simulation tool QUOKKA3. This analysis identifies the optical losses as the most severe ones. Based on this loss analysis, a possible pathway for an efficiency of 25% using nc-SiC:H(n) front contacts is designed, where the biggest gains in efficiency come from a reduced front finger width and a reduced recombination velocity at the front c-Si surface from a better passivation. When halving the finger width, adjusting the finger pitch and, based on Sentaurus TCAD simulations, reducing the thickness of the ITO while adding a silicon nitride layer as additional ARC, a $J_{SC} > 42$ mA cm^{-2} could be achieved.

5. Experimental Section

The fabrication of the certified cells was described elsewhere,[11] but a short introduction was given in the Supporting Information. The *EQE*, reflectance (*R*) curves, and IV parameters were measured with the LOANA system from pv-tools GmbH under standard test conditions. The implied V_{OC} (iV_{OC}) and pseudo FF (*pFF*), which is the *FF* without contributions from resistive effects, were measured with a Sinton WTC-120 lifetime tester in quasi steady-state conditions. The reflectance curve used as input for QUOKKA3 was simulated using the freeware tool OPAL2,[30–32] the road map was designed using the software QUOKKA3,[33–36] and the J_{SC} optimization was done using the software Sentaurus TCAD. In the Sentaurus TCAD simulations, ray tracing with transfer matrix method boundaries was applied to simulate the optical response of the device. The optical properties of the involved materials were taken from spectroscopic ellipsometry measurements and the layer thicknesses were adjusted to achieve the best agreement with measured EQE. The optical simulation results were then used as an input for the electrical simulation of the device. A 2D input optical generation profile was calculated from the total photon absorption in a c-Si layer of the 3D optical simulation result. In the 2D electrical device simulation, a nonlocal tunneling model, as implemented in Sentaurus TCAD, was used to model the carrier transport through tunneling thin oxide layer, whereas for the rear side, that is, amorphous silicon and ITO contact, band-to-band tunneling was considered. Furthermore, a contribution of trap-assisted tunneling was included in amorphous silicon layers. The implemented 2D electrical device model had given a good agreement with experiment for the certified 24% cell.

Further details on the simulation model setup and parameters used can be found in literature.[37] Note that for this work measured electrical conductivity (σ) of the passivation and conductive silicon carbide layers, 5E-09 S cm^{-1} and 5 E-01 S cm^{-1}, respectively, were used. And, tunneling effective masses used for the oxide barrier were $0.4 * m_0$ and $0.32 * m_0$ for electrons and holes, respectively, as in literature.[38] m_0 stood for the rest mass of an electron. The initial optical loss analysis was performed using a method proposed by Paviet-Salomon et al.[15]

Supporting Information

Supporting Information is available from the Wiley Online Library or from the author.

Acknowledgements

The authors gratefully acknowledge the funding of the German Federal Ministry of Economic Affairs and Energy in the framework of the TUKAN project (grant: 0324198D). The work of A.Z. was supported in part by the German Academic Exchange Service (DAAD) and in part by the Ministry of Science and Higher Education of the Russian Federation, under Project 3.13378.2019/13.2.

Open access funding enabled and organized by Projekt DEAL.

Conflict of Interest

The authors declare no conflict of interest.

Data Availability Statement

The data that support the findings of this study are available from the corresponding author upon reasonable request.

Keywords

antireflective coatings, magnesium fluoride, passivating contacts, silicon carbides, silicon solar cells

Received: December 9, 2021
Revised: January 27, 2022
Published online: February 9, 2022

[1] S. W. Glunz, B. Steinhauser, J. I. Polzin, C. Luderer, B. Grübel, T. Niewelt, A. M. O. M. Okasha, M. Bories, H. Nagel, K. Krieg, F. Feldmann, A. Richter, M. Bivour, M. Hermle, *Progr. Photovoltaics: Res. Applic.* **2021**.
[2] W. Duan, A. Lambertz, K. Bittkau, D. Qiu, K. Qiu, U. Rau, K. Ding, *Progr. Photovoltaics: Res. Applic.* **2021**.
[3] Z. C. Holman, A. Descoeudres, L. Barraud, F. Z. Fernandez, J. P. Seif, S. De Wolf, C. Ballif, *IEEE J. Photovoltaics* **2012**, *2*, 7.
[4] S. Reiter, N. Koper, R. Reineke-Koch, Y. Larionova, M. Turcu, J. Krügener, D. Tetzlaff, T. Wietler, U. Höhne, J.-D. Kähler, *Energy Procedia* **2016**, *92*, 199.
[5] T. G. Allen, J. Bullock, X. B. Yang, A. Javey, S. De Wolf, *Nat. Energy* **2019**, *4*, 914.
[6] K. Sopian, S. L. Cheow, S. H. Zaidi, in *4th Int. Conf. on the Advancement of Materials and Nanotechnology (Icamn Iv 2016)*, AIP Publishing LLC vol. *1877*, **2017**, p. 020004.
[7] A. Louwen, W. van Sark, R. Schropp, A. Faaij, *Sol. Energy Mater. Sol. Cells* **2016**, *147*, 295.
[8] Y. Q. Liu, Y. J. Li, Y. L. Wu, G. T. Yang, L. Mazzarella, P. Procel-Moya, A. C. Tamboli, K. Weber, M. Boccard, O. Isabella, X. B. Yang, B. Q. Sun, *Mater. Sci. Eng. R-Rep.* **2020**, *142*, 100579.
[9] G. Nogay, J. P. Seif, Y. Riesen, A. Tomasi, Q. Jeangros, N. Wyrsch, F. J. Haug, S. De Wolf, C. Ballif, *IEEE J. Photovoltaics* **2016**, *6*, 1654.
[10] J. P. Seif, A. Descoeudres, G. Nogay, S. Hanni, S. M. de Nicolas, N. Holm, J. Geissbuhler, A. Hessler-Wyser, M. Duchamp, R. E. Dunin-Borkowski, M. Ledinsky, S. De Wolf, C. Ballif, *IEEE J. Photovoltaics* **2016**, *6*, 1132.
[11] M. Köhler, M. Pomaska, P. Procel, R. Santbergen, A. Zamchiy, B. Macco, A. Lambertz, W. Duan, P. Cao, B. Klingebiel, S. Li, A. Eberst, M. Luysberg, K. Qiu, O. Isabella, F. Finger, T. Kirchartz, U. Rau, K. Ding, *Nat. Energy* **2021**, *6*, 529.

© 2022 The Authors. Solar RRL published by Wiley-VCH GmbH

2367198x, 2022, 6, Downloaded from https://onlinelibrary.wiley.com/doi/10.1002/solr.202101050 by Universitatsbibliothek RWTH Aachen University, Wiley Online Library on [19/02/2026]. See the Terms and Conditions (https://onlinelibrary.wiley.com/terms-and-conditions) on Wiley Online Library for rules of use; OA articles are governed by the applicable Creative Commons License

[12] M. Kohler, M. Pomaska, F. Lentz, F. Finger, U. Rau, K. Ding, *ACS Appl. Mater. Interfaces* **2018**, *10*, 14259.
[13] M. Köhler, A. Zamchiy, M. Pomaska, A. Lambertz, F. Lentz, W. Duan, V. Smirnov, F. Finger, U. Rau, K. Ding, in *2018 IEEE 7th World Conf. on Photovoltaic Energy Conversion (WCPEC) (A Joint Conf. of 45th IEEE PVSC, 28th PVSEC & 34th EU PVSEC)*, IEEE, Waikoloa, HI, USA **2018**, p. 3468.
[14] M. Kohler, M. Pomaska, A. Zamchiy, A. Lambertz, W. Duan, F. Lentz, S. Li, V. Smirnov, T. Kirchartz, F. Finger, U. Rau, K. Ding, *IEEE J. Photovoltaics* **2020**, *10*, 46.
[15] B. Paviet-Salomon, A. Tomasi, A. Descoeudres, L. Barraud, S. Nicolay, M. Despeisse, S. De Wolf, C. Ballif, *IEEE J. Photovoltaics* **2015**, *5*, 1293.
[16] A. Cruz Bournazou, *Transparent Conductive Oxides for Silicon Heterojunction Solar Cells: Interaction between Materials and Device*, Technische Universität Berlin, Berlin, Germany. Dissertation **2020**.
[17] M. A. Leilaeioun, *Fill Factor Loss Mechanisms: Analysis and Basic Understanding in Silicon Hetero-junction Solar Cells*, Arizona State University, Tempe, Arizona, USA. Dissertation **2018**.
[18] O. Kabadayi, H. Gumus, *Phys. Status Solidi B-Basic Solid State Phys.* **2005**, *242*, 2391.
[19] A. Duncanson, R. W. H. Stevenson, *Proc. Phys. Soc. Lond.* **1958**, *72*, 1001.
[20] B. Dorner, H. Schober, A. Wonhas, M. Schmitt, D. Strauch, *Eur. Phys. J. B* **1998**, *5*, 839.
[21] W. Beyer, U. Zastrow, *J. Non-Cryst. Solids* **2000**, *266*, 206.
[22] W. B. Jackson, N. M. Johnson, C. C. Tsai, I. W. Wu, A. Chiang, D. Smith, *Appl. Phys. Lett.* **1992**, *61*, 1670.
[23] N. H. Nickel, W. B. Jackson, I. W. Wu, C. C. Tsai, A. Chiang, *Phys. Rev. B Condens. Matter* **1995**, *52*, 7791.
[24] A. Moldovan, F. Feldmann, K. Kaufmann, S. Richter, M. Wemer, C. Hagendorf, M. Zimmer, L. Rentsch, M. Hermle, in *2015 IEEE 42nd Photovoltaic Specialist Conf. (PVSC)*, IEEE, New Orleans, LA, USA **2015**.
[25] A. Moldovan, F. Feldmann, G. Krugel, M. Zimmer, J. Rentsch, M. Hermle, A. Roth-Folsch, K. Kaufmann, C. Hagendorf, in *Proc. of the 4th Int. Conf. on Crystalline Silicon Photovoltaics (Siliconpv 2014)*, Elsevier, vol. *55*, **2014**, p. 834.
[26] M. Boccard, N. Rodkey, Z. C. Holman, in *Proc. of the 6th Int. Conf. on Crystalline Silicon Photovoltaics (Siliconpv 2016)*, Vol. *92*, **2016**, p. 297.
[27] S. Nunomura, I. Sakata, A. Sato, M. Lozac'h, T. Misawa, N. Itagaki, M. Shiratani, *J. Phys. Chem. Solids* **2021**, *156*, https://doi.org/10.1016/j.jpcs.2021.110127.
[28] M. Pomaska, J. Mock, F. Köhler, U. Zastrow, M. Perani, O. Astakhov, D. Cavalcoli, R. Carius, F. Finger, K. Ding, *J. Appl. Phys.* **2016**, *120*, 225105.
[29] S. Li, M. Pomaska, A. Lambertz, W. Duan, K. Bittkau, D. Qiu, Z. Yao, M. Luysberg, P. Steuter, M. Köhler, *Joule* **2021**, *5*, 1535.
[30] S. C. Baker-Finch, K. R. McIntosh, *Progr. Photovoltaics* **2011**, *19*, 406.
[31] S. C. Baker-Finch, K. R. McIntosh, in *35th IEEE Photovoltaic Specialists Conf.*, IEEE, Honolulu, HI, USA **2010**, p. 2184.
[32] K. R. McIntosh, S. C. Baker-Finch, in *2012 38th IEEE Photovoltaic Specialists Conf. (Pvsc)*, IEEE, Austin, TX, USA **2012**, p. 265.
[33] A. Fell, P. P. Altermatt, *IEEE J. Photovoltaics* **2018**, *8*, 1443.
[34] A. Fell, K. R. McIntosh, K. C. Fong, *IEEE J. Photovoltaics* **2016**, *6*, 611.
[35] A. Fell, J. Schon, M. Muller, N. Wohrle, M. C. Schubert, S. W. Glunz, *IEEE J. Photovoltaics* **2018**, *8*, 428.
[36] A. Fell, J. Schon, M. C. Schubert, S. W. Glunz, *Solar Energy Mater. Solar Cells* **2017**, *173*, 128.
[37] H. T. Gebrewold, K. Bittkau, K. Qiu, K. Ding, in *2021 IEEE 48th Photovoltaic Specialists Conf. (PVSC)*, IEEE, Fort Lauderdale, FL, USA **2021**, p. 1115.
[38] P. Procel, P. Löper, F. Crupi, C. Ballif, A. Ingenito, *Solar Energy Mater. Solar Cells* **2019**, *200*, 109937.

© 2022 The Authors. Solar RRL published by Wiley-VCH GmbH

2367198x, 2022, 6, Downloaded from https://onlinelibrary.wiley.com/doi/10.1002/solr.202101050 by Universitatsbibliothek RWTH Aachen University, Wiley Online Library on [19/02/2026]. See the Terms and Conditions (https://onlinelibrary.wiley.com/terms-and-conditions) on Wiley Online Library for rules of use; OA articles are governed by the applicable Creative Commons License